

# Room temperature oxidation of acetone by ozone over alumina-supported manganese and cobalt mixed oxides

Mehran Ghavami<sup>1</sup>, Mostafa Aghbolaghy<sup>1</sup>, Jafar Soltan (✉)<sup>1</sup>, Ning Chen<sup>1,2</sup>

<sup>1</sup> Department of Chemical and Biological Engineering, University of Saskatchewan, Saskatoon, S7N 5A9, Canada

<sup>2</sup> Canadian Light Source Inc., University of Saskatchewan, Saskatoon, S7N 0X4, Canada

© Higher Education Press 2020

**Abstract** Volatile organic compounds (VOCs) are among the major sources of air pollution. Catalytic ozonation is an efficient process for removing VOCs at lower reaction temperature compared to catalytic oxidation. In this study, a series of alumina supported single and mixed manganese and cobalt oxides catalysts were used for ozonation of acetone at room temperature. The influence of augmenting the single Mn and Co catalysts were investigated on the performance and structure of the catalyst. The manganese and cobalt single and mixed oxides catalysts of the formula Mn10%-CoX and Co10%-MnX (where X = 0, 2.5%, 5%, or 10%) were prepared. It was found that addition of Mn and Co at lower loading levels (2.5% or 5%) to single metal oxide catalysts enhanced the catalytic activity. The mixed oxides catalysts of (Mn10%-Co2.5%) and (Mn10%-Co5%) led to acetone conversion of about 84%. It is concluded that lower oxidation state of the secondary metal improves ozone decomposition and oxidation of acetone.

**Keywords** ozone, VOC, manganese oxides, cobalt oxides, alumina support

## 1 Introduction

Air pollution by volatile organic compounds (VOCs) is an environmental threat that can negatively affect human health [1,2]. Ozone is considered a strong oxidant for water treatment and air cleaning [3,4]. Catalytic reaction with ozone (catalytic ozonation) is a promising method for VOC removal with distinct advantages over catalytic oxidation processes. Important advantages of catalytic ozonation are oxidation of VOCs at lower temperature, the

possibility of using transition metal oxides catalysts instead of noble metals, and effectiveness of the process at low concentration levels of the VOC [5–8].

Transition metal oxides such as Mn, Co, Cu, Ni, Fe, and Ce are among the most active metals in catalytic ozonation reactions [9]. Supported manganese oxides are the most effective catalysts for oxidation of VOCs with ozone [10–13]. It has been reported that high activity of MnO<sub>x</sub> in the oxidation of VOCs can be related to the activity of Mn in decomposition of ozone and generation of active oxygen species [14]. VOC removal rates normalized by catalyst surface area were determined to be higher for alumina-supported catalysts than titania, silica, or zirconia-supported catalysts [15]. Investigation on catalytic ozonation of acetone using supported manganese oxide catalyst on  $\gamma$ -alumina and silica showed that alumina-supported catalyst was more active than the silica-supported catalyst in acetone removal [10].

One method of enhancing the catalyst activity is the addition of another metal to the supported manganese oxide. It has been reported that mixed metal catalysts can offer higher catalytic performance and selectivity, and better deactivation resistance compared to monometallic catalysts [16–18]. Among transition metal oxides, cobalt oxides have been identified as promising catalysts in oxidation of VOCs [16,19–21]. Doping ceria with cobalt oxide has been reported to modify the redox properties, enhance the oxygen mobility and eventually lead to better catalyst activity [20,22]. Cobalt is a metal with different oxidation states and relatively low energy gap exists between its different oxidation states. This can be beneficial for ozone decomposition and catalytic ozonation reactions [23].

In the present study, alumina supported Mn and Co single and mixed metal catalysts with different loadings of Co or Mn were used in catalytic ozonation of acetone at room temperature. The model VOC in this work was acetone since it is a prevalent industrial solvent and

common pollutant in indoor air [10]. Reed et al. examined ozonation of acetone on silica-supported manganese oxide catalysts. The effect of metal oxide loading on oxidation of acetone was investigated, and it was noted that higher Mn loadings of silica-supported catalysts are more active due to their lower oxidation state and better adsorption of intermediates and easier delivery of oxygen equivalents [14]. On the contrary, it has also been reported that lower loadings of Mn are more favorable in catalytic ozonation of VOCs due to higher dispersion of Mn as well as lower oxidation states of Mn [11,12,24]. Einaga et al. [25] investigated the effect of different metal oxides of Fe, Co, Ni, and Cu on performance of unsupported Mn catalyst based on the catalyst activity and selectivity in oxidation of benzene with ozone. They reported that Co-Mn mixed oxide was the most effective catalyst for benzene oxidation among the mixed oxide catalysts. Yao et al. [26] applied post plasma catalysis system to remove hexanal at ambient temperature and pressure from air using unsupported Co-Mn catalyst with different mole ratios. They deduced that CoMn(9/1) showed the best catalytic activity because the redox properties of Co-Mn solid solutions were promoted. Since both Mn and Co are active metals in catalytic ozonation of VOCs, catalytic ozonation of acetone over alumina supported Mn and Co mixed oxide catalysts at different levels of the primary and secondary metal loading was investigated. The catalysts were characterized by Brunauer-Emmet-Teller (BET) surface area and pore volume, X-ray diffraction (XRD), X-ray absorption near edge structure (XANES), extended X-ray absorption fine structure (EXAFS), and diffuse reflectance infrared Fourier transform spectroscopy (DRIFT) to relate the properties of the catalysts to their activities.

## 2 Experimental

### 2.1 Catalyst preparation

Single  $\text{MnO}_x$  and  $\text{CoO}_x$  catalysts with metal loading of 10 wt-% on  $\gamma\text{-Al}_2\text{O}_3$  (Alfa Aesar,  $S_{\text{BET}} = 220 \text{ m}^2 \cdot \text{g}^{-1}$ ) were prepared by dry impregnation method using manganese (II) nitrate tetrahydrate (Sigma-Aldrich, 97%) and cobalt (II) nitrate hexahydrate (Sigma-Aldrich, 98%) precursors. After impregnation by the given amounts of the precursor solution, catalysts were dried at  $100^\circ\text{C}$  for 10 h and calcined at  $500^\circ\text{C}$  for 4 h. The calcined catalysts were crushed and sieved to achieve particles with diameter less than  $208 \mu\text{m}$  for activity tests.

The mixed transition metal oxides catalysts were prepared via successive impregnation method. Once the single metal catalysts were prepared, Mn-Co mixed oxides catalysts were synthesized by adding 2.5, 5, and 10 wt-% Co to the already prepared  $\text{MnO}_x/\gamma\text{-Al}_2\text{O}_3$  catalyst using cobalt (II) nitrate hexahydrate solution. In the case of Co-Mn catalysts, solutions of manganese (II) nitrate

tetrahydrate with appropriate content were added to the already prepared  $\text{CoO}_x/\gamma\text{-Al}_2\text{O}_3$  catalyst. The catalysts were dried, calcined, and sieved again.

### 2.2 Catalyst characterization

BET surface area and pore volume of the catalysts were determined by nitrogen adsorption using ASAP 2020 (Micromeritics) instrument. The samples were degassed for 2 h at  $110^\circ\text{C}$  and 66.7 Pa before the surface area and pore volume measurements. Structure of the catalysts was analyzed by XRD, XANES, and EXAFS. XRD spectra were collected by Bruker diffractometer (D8 Advance, Cu  $K\alpha$  radiation) in the  $2\theta$  range of  $10^\circ\text{--}80^\circ$  with a step size of  $0.04^\circ$ . XANES and EXAFS spectra of Mn K-edge and Co K-edge were collected at HXMA beamline of the Canadian Light Source. Catalysts were diluted with boron nitride, ground, and pressed to make thin disks. The prepared disks were protected by Kapton tape. All measurements were carried out in transmission mode using straight ion chamber detectors filled with helium gas. A Si(1 1 1) monochromator crystal used for data collection and the beamline was operated in Rh mirrors. Data processing was performed by ATHENA software [27].

### 2.3 Experimental setup and activity tests

A schematic diagram of the experimental setup is shown in Fig. 1. An ozone generator (AZCO Industries LTD, HTU-500S) was used to generate ozone from a high purity oxygen cylinder (Praxair, 99.993%). An acetone cylinder with ppm level concentration (Praxair, accuracy of  $\pm 2\%$ ) was diluted with nitrogen (Praxair, 99.999%) to provide acetone with appropriate concentration in the system. Gas flows were controlled by mass flow controllers (Brooks, SLA 5850, accuracy of  $\pm 1\%$ ). The catalytic ozonation experiments were carried out at  $25^\circ\text{C}$  and atmospheric pressure using a feed gas with 1200 ppm ozone and 150 ppm acetone.

Total feed flow rate of  $250 \text{ mL} \cdot \text{min}^{-1}$  (at standard atmospheric pressure) was set for all experiments. For each experiment, 0.065 g of the fresh catalyst was used. First, feed gas streams passed through a horizontal Pyrex tube, filled with glass beads, to enhance mixing before entering the reactor. All the reaction experiments were conducted in a reaction chamber (Harrick, HVC) at atmospheric pressure. Concentration of ozone was measured by an ozone analyzer (Teledyne API M454) in the exhaust gas stream. A long-path gas cell (PIKE, volume 0.1 L, 2.4 m optical length, KBr window) coupled with a Nicolet iS50 Fourier transform infrared (FTIR) spectrometer equipped with a Deuterated L-alanine doped triglycine sulfate detector was used for analysis of acetone, CO, and  $\text{CO}_2$ . Based on the blank tests, homogeneous reaction between ozone and acetone in the absence of the catalyst was negligible in this system.

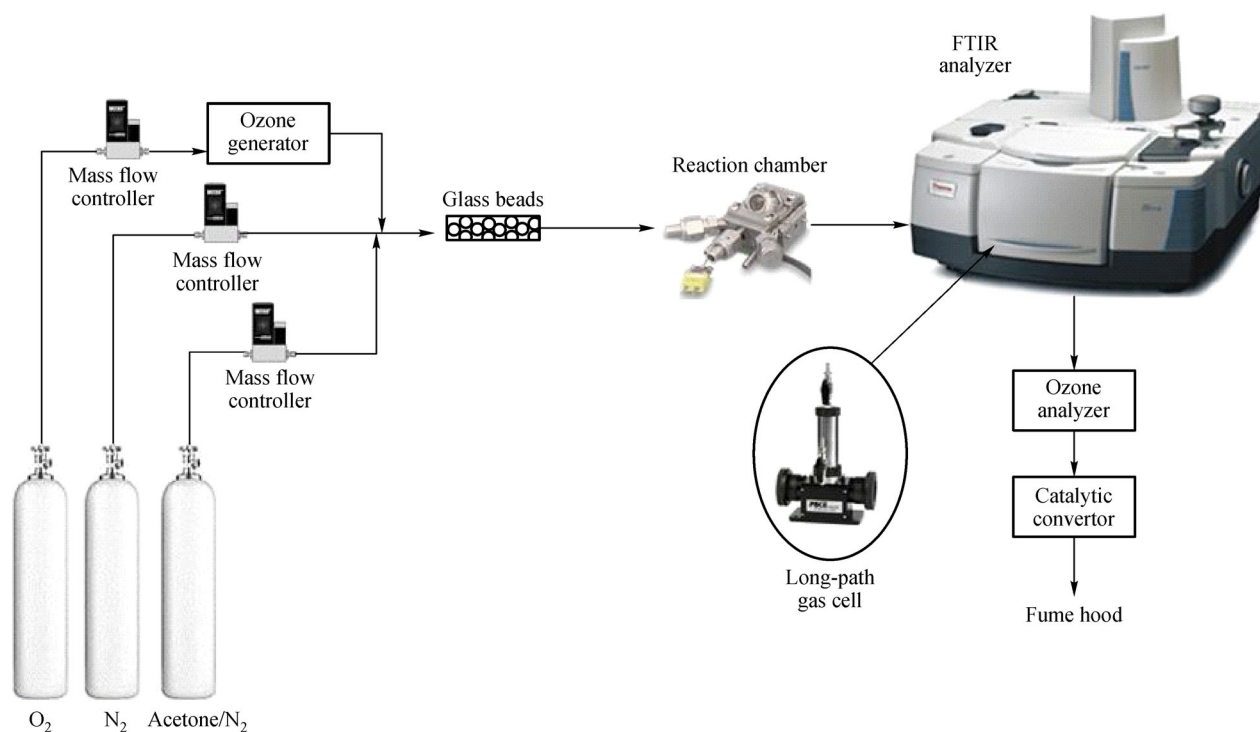


Fig. 1 Schematic of the experimental setup.

Prior to the reaction, the catalyst was heated for 1 h under flow of  $200 \text{ mL} \cdot \text{min}^{-1}$  oxygen at  $490^\circ\text{C}$ . Then, the catalyst was cooled down to the reaction temperature under  $250 \text{ mL} \cdot \text{min}^{-1}$  nitrogen flow. The catalyst was saturated by passing gas mixture containing acetone, nitrogen, and oxygen before introducing ozone to the reaction chamber. After the catalyst became saturated with acetone, the ozone generator was turned on, and the ozonation of acetone was monitored at room temperature for 150 min. Experiments were repeated, and experimental errors in terms of standard error were calculated. For calibration purposes, a gas cylinder with ppm level concentrations of carbon dioxide and carbon monoxide balanced with nitrogen (Praxair, accuracy of  $\pm 2\%$ ) was used.

DRIFTS studies was performed in another configuration of the experimental setup in which the long-path gas cell was replaced with a DRIFTS accessory (Harrick, Praying Mantis) on the FTIR spectrometer. The reaction chamber, equipped with ZnSe windows, was installed in the DRIFTS accessory in the FTIR spectrometer. To attain higher sensitivity and faster scanning, a narrow band mercuric cadmium telluride (MCT-A) detector was used for the DRIFTS operations. Spectra were collected at a resolution of  $4 \text{ cm}^{-1}$  in the range of  $3900\text{--}1300 \text{ cm}^{-1}$  to avoid saturation of the MCT-A detector. The acetone and ozone conversions ( $X_i$ ) were calculated as follows:

$$X_i = \frac{c_{i,\text{in}} - c_{i,\text{out}}}{c_{i,\text{in}}} \times 100\%, \quad (1)$$

where  $C_{i,\text{in}}$  and  $C_{i,\text{out}}$  are the inlet and outlet concentrations of acetone or ozone, respectively.  $\text{CO}_x$  yield was calculated from the following equation:

$$\text{CO}_x \text{ yield}(\%) = \frac{[\text{CO}] + [\text{CO}_2]}{3 \times [\text{C}_3\text{H}_6\text{O}]_{\text{reacted}}} \times 100. \quad (2)$$

## 3 Results and discussion

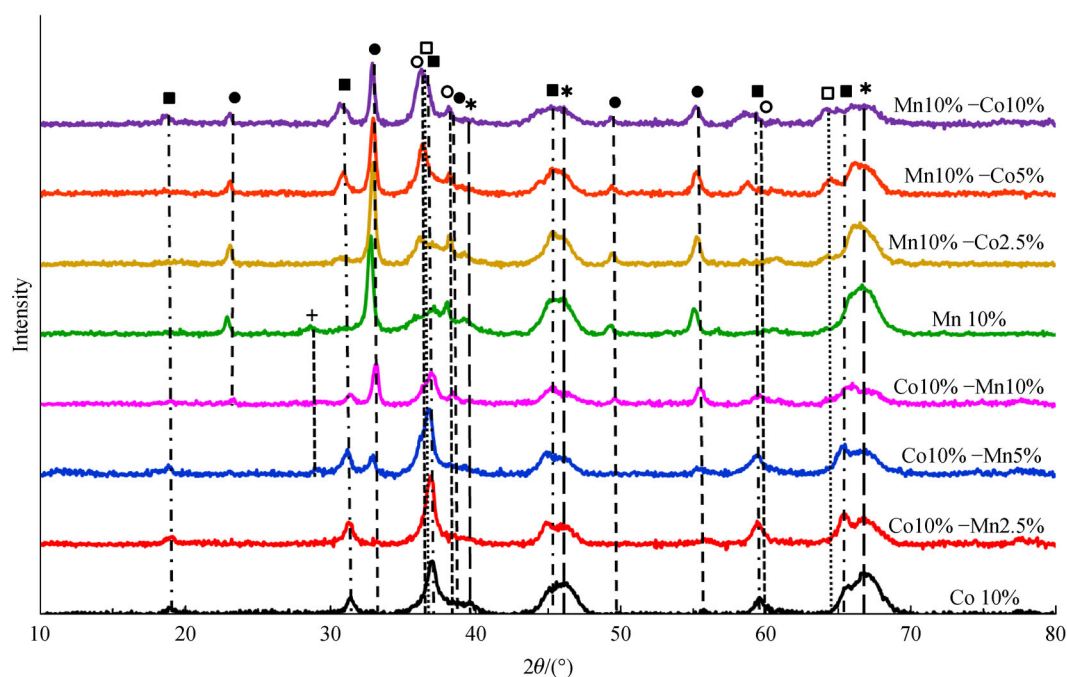
### 3.1 Catalyst characterization

Table 1 presents Mn and Co loading, BET surface area, and pore volume of all the studied catalysts and the alumina support. By adding Mn and Co on the alumina, surface area and pore volume of the samples decreased. In the mixed oxide catalysts, surface area and pore volume kept decreasing by increasing metal loading mainly due to contribution of the mass of nonporous metal components to the catalyst mass and partial plugging of alumina pores [12].

Figure 2 shows XRD spectra of the eight catalysts supported on alumina. According to XRD peaks,  $\text{Mn}_2\text{O}_3$  and  $\text{Co}_3\text{O}_4$  are the main phases of manganese and cobalt oxides in single metal oxides catalysts [28,29].  $\text{Co}_3\text{O}_4$  has a sharp peak at  $37^\circ$ , which can be observed in all catalysts containing cobalt. In  $\text{CoO}_x/\gamma\text{-Al}_2\text{O}_3$ , only peaks related to  $\text{Co}_3\text{O}_4$  phase can be seen. In Co-based catalysts augmented

**Table 1** Chemical compositions and pore structures of the catalysts

Catalyst	Mn and Co loading /wt-%		$S_{\text{BET}} / (\text{m}^2 \cdot \text{g}^{-1})$	Pore volume $/( \text{cm}^3 \cdot \text{g}^{-1} )$
	Mn	Co		
$\gamma\text{-Al}_2\text{O}_3$	–	–	220	0.61
Mn/ $\gamma\text{-Al}_2\text{O}_3$	10	–	200	0.56
Mn-Co/ $\gamma\text{-Al}_2\text{O}_3$	10	2.5	186	0.54
Mn-Co/ $\gamma\text{-Al}_2\text{O}_3$	10	5	178	0.53
Mn-Co/ $\gamma\text{-Al}_2\text{O}_3$	10	10	180	0.49
Co/ $\gamma\text{-Al}_2\text{O}_3$	–	10	210	0.59
Co-Mn/ $\gamma\text{-Al}_2\text{O}_3$	2.5	10	194	0.55
Co-Mn/ $\gamma\text{-Al}_2\text{O}_3$	5	10	183	0.52
Co-Mn/ $\gamma\text{-Al}_2\text{O}_3$	10	10	174	0.47

**Fig. 2** XRD patterns of the alumina supported catalysts ( $\text{Al}_2\text{O}_3$  \*,  $\text{Mn}_2\text{O}_3$  ●,  $\text{Mn}_3\text{O}_4$  ○,  $\text{MnO}_2$  +,  $\text{Co}_3\text{O}_4$  ■,  $\text{CoO}$  □).

by adding different loadings of manganese, the main phase of cobalt oxides is  $\text{Co}_3\text{O}_4$ . Whereas, in Mn-based catalysts augmented by adding cobalt, an overlap of  $\text{Co}_3\text{O}_4$  and  $\text{CoO}$  peaks can be observed. In  $\text{MnO}_x/\gamma\text{-Al}_2\text{O}_3$  sample, different phases of manganese oxide can be observed in the XRD spectra. The most intense peak of  $\text{Mn}_3\text{O}_4$  is located at  $36.2^\circ$ , which is hardly recognizable due to the overlap of the peak with that of  $\text{Co}_3\text{O}_4$ .

Therefore, XRD spectra of the catalysts indicate that with change in the loading of the secondary metal, different phases of Mn and Co oxides are formed, while the oxidation state of the primary metal in the catalyst remains unchanged. From the XRD peaks, metal oxide crystallite sizes were estimated by using the Scherrer

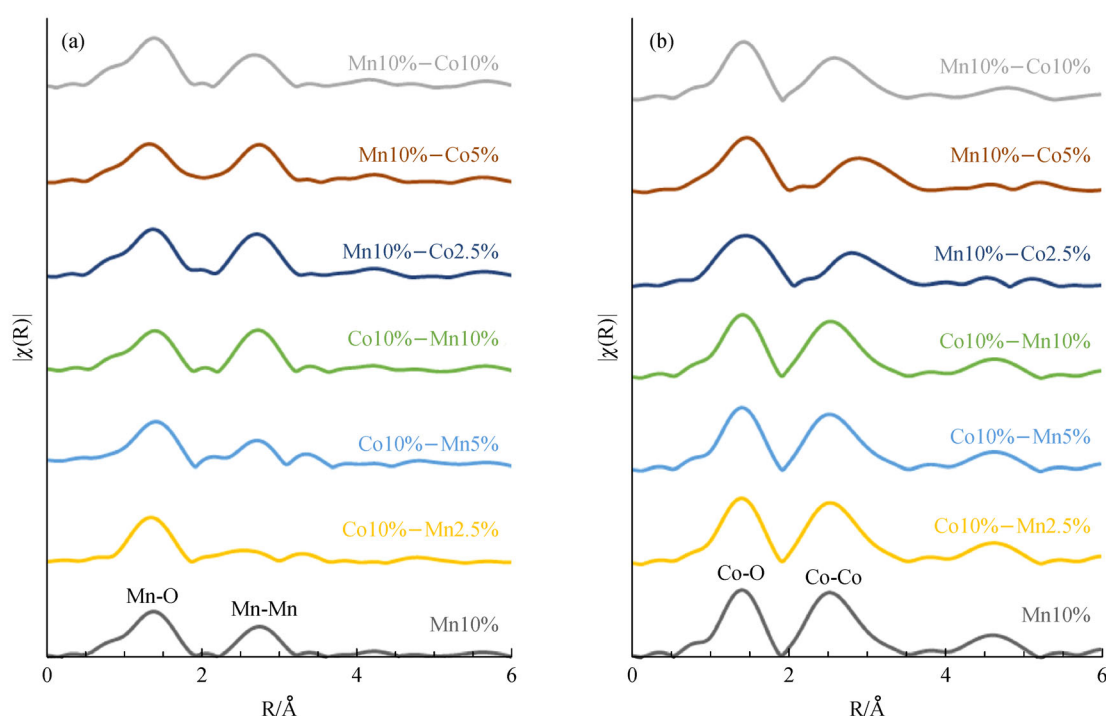
equation. Particle size of  $\text{Mn}_2\text{O}_3$  is determined from XRD spectra using the most intense peak at  $32.9^\circ$  [30].  $\text{Co}_3\text{O}_4$  metal crystallite size was determined from XRD spectra using the  $\text{Co}_3\text{O}_4$  peak at  $2\theta$  value of  $31.4^\circ$ . It was determined that  $\text{Mn}_2\text{O}_3$  had crystallite size between 18 and 26 nm, whereas  $\text{Co}_3\text{O}_4$  crystallites fall in the range of 9 and 21 nm size range. Catalyst dispersion values were estimated from the obtained particle sizes calculated from XRD peak broadening [31,32]. Table 2 presents  $\text{Co}_3\text{O}_4$  and  $\text{Mn}_2\text{O}_3$  crystallite size and dispersion values obtained from XRD spectra. The results indicate no specific correlation between the loading of the secondary metal and dispersion of the metals on the catalysts.

Figure 3(a) shows the magnitude of the Fourier trans-

**Table 2** Mn and Co oxides particle sizes and dispersions obtained from XRD spectra

Catalyst	Mn <sub>2</sub> O <sub>3</sub> particle size /nm	Mn dispersion /%	Co <sub>3</sub> O <sub>4</sub> particle size /nm	Co dispersion /%
Mn10%/γ-Al <sub>2</sub> O <sub>3</sub>	18	7	–	–
Mn10%-Co2.5%/γ-Al <sub>2</sub> O <sub>3</sub>	26	5	N <sup>a)</sup>	N <sup>a)</sup>
Mn10%-Co5%/γ-Al <sub>2</sub> O <sub>3</sub>	20	7	13	5
Mn10%-Co10%/γ-Al <sub>2</sub> O <sub>3</sub>	23	6	9	7
Co10%/γ-Al <sub>2</sub> O <sub>3</sub>	–	–	14	4
Co10%-Mn2.5%/γ-Al <sub>2</sub> O <sub>3</sub>	N <sup>a)</sup>	N <sup>a)</sup>	21	3
Co10%-Mn5%/γ-Al <sub>2</sub> O <sub>3</sub>	18	7	12	5
Co10%-Mn10%/γ-Al <sub>2</sub> O <sub>3</sub>	18	7	12	5

a) Not detected

**Fig. 3** Magnitude of the Fourier transform of EXAFS spectra: (a) Mn K-edge, (b) Co K-edge.

form of Mn K-edge of the catalysts. The peak for Mn-O in the first coordination shell is similar for all the catalysts containing manganese oxide. However, the peak for Mn-Mn in the second coordination shell of Co10%-Mn2.5% and Co10%-Mn5% is different from that of the other catalysts. In other words, local structure around manganese atom is similar for all the manganese-containing catalysts except for the catalysts with 2.5% and 5% manganese loading.

Figure 3(b) shows the magnitude of the Fourier transform of Co K-edge EXAFS spectra of the catalysts. The first coordination shell (Co-O) is similar for all cobalt-containing catalysts. However, the peak for Co-Co in the second shell of Mn10%-Co2.5% and Mn10%-Co5% has

shifted when compared to the Co-Co peak of the other catalysts. Therefore, the catalysts with 2.5% and 5% cobalt loading have different local structure around cobalt atom than the other cobalt-containing catalysts.

Table 3 shows the presence of different phases of manganese oxide and cobalt oxide in the catalysts. These results were obtained from linear combination fitting of Mn K-edge and Co K-edge XANES spectra. Mn<sub>2</sub>O<sub>3</sub> is the dominant manganese phase in the catalysts that contain 10% manganese. Addition of cobalt to Mn10% catalyst did not change the formal oxidation state of manganese significantly. In contrast, Mn<sub>3</sub>O<sub>4</sub> was the main manganese phase in the Co10%-Mn2.5% and Co10%-Mn5% catalysts. Increase in manganese loading decreased Mn<sub>3</sub>O<sub>4</sub> and

**Table 3** Result of linear combination fitting of Mn and Co K-edge XANES

Catalyst	Mn <sub>3</sub> O <sub>4</sub> /%	Mn <sub>2</sub> O <sub>3</sub> /%	MnO <sub>2</sub> /%	CoO /%	Co <sub>3</sub> O <sub>4</sub> /%
Mn10%/γ-Al <sub>2</sub> O <sub>3</sub>	7	82	11	–	–
Mn10%-Co2.5%/γ-Al <sub>2</sub> O <sub>3</sub>	20	80	0	45	55
Mn10%-Co5%/γ-Al <sub>2</sub> O <sub>3</sub>	16	84	0	44	56
Mn10%-Co10%/γ-Al <sub>2</sub> O <sub>3</sub>	7	85	8	16	84
Co10%/γ-Al <sub>2</sub> O <sub>3</sub>	–	–	–	–	100
Co10%-Mn2.5%/γ-Al <sub>2</sub> O <sub>3</sub>	69	29	2	–	100
Co10%-Mn5%/γ-Al <sub>2</sub> O <sub>3</sub>	54	44	2	2	98
Co10%-Mn10%/γ-Al <sub>2</sub> O <sub>3</sub>	27	73	0	3	97

increased Mn<sub>2</sub>O<sub>3</sub> content of the Co-Mn catalysts. Co<sub>3</sub>O<sub>4</sub> is the dominant cobalt phase of the cobalt-containing catalysts except for Mn10%-Co2.5% and Mn10%-Co5% that contain significant amount of CoO phase as well. Addition of manganese to Co10% catalyst did not alter the formal oxidation state of cobalt.

Results obtained from XANES and XAFS analyses show that the local structure and oxidation state of transition metals (Mn or Co) formed during the first impregnation of the alumina remain unchanged even after addition of the secondary metal. In other words, Mn<sub>2</sub>O<sub>3</sub> was the main manganese phase of Mn10%, and adding cobalt did not affect the manganese phase. Similarly, Co<sub>3</sub>O<sub>4</sub> was the main cobalt phase of Co10%, and adding manganese did not influence the cobalt phase. On the other hand, as found by XANES, the oxidation states of the secondary metal changed, and by increasing the loading of the secondary metal, its oxidation state increased. This agrees with the XRD results. The direct relationship between manganese loading and oxidation state has also been reported by Rezaei et al. [12].

### 3.2 Catalytic oxidation of acetone by ozone

Catalytic ozonation of acetone using single and mixed transition metal oxide catalysts was conducted at 25°C. Figure 4 depicts acetone and ozone conversions using the eight catalysts at 150 min of the reaction. Acetone and ozone conversions increased by augmenting the Mn and Co-based catalysts with the secondary metal. However, the activity of the catalysts decreases as the loading of the secondary metal increases up to 10%. The order of adding metals in the catalyst preparation changed the catalytic properties. It can be observed that generally, Mn-based catalysts augmented by Co are more active than Co-based catalysts that are augmented by Mn. Mn oxides augmented with lower loading of Co showed the highest activity for the reaction. Both Mn10%-Co2.5% and Mn10%-Co5% catalysts achieved acetone conversion of approximately 84%. For Co-based catalyst, as Mn content increased, the catalyst activity kept decreasing. By adding appropriate

content of Co to Mn-based catalyst, the acetone and ozone conversions increased by 26% and 54%, respectively. The results indicate about 53% and 52% increase in acetone and ozone conversions by augmenting single Co catalyst with proper amount of Mn. Table 4 shows the reaction rates of acetone and ozone conversions on all studied catalysts. It can be observed that Mn10%-Co2.5% and Mn10%-Co5% had the highest acetone and ozone reaction rates.

The main reaction products of catalytic ozonation of acetone are CO and CO<sub>2</sub>. The CO<sub>x</sub> yields were determined for all catalysts and are shown in Table 4. CO<sub>x</sub> yields for ozonation of acetone for all the catalysts were between 88% and 97%. The percentage of CO and CO<sub>2</sub> in the exhaust gas is presented in Fig. 5. It should be mentioned that the results of CO<sub>x</sub> yield and percentages of CO and CO<sub>2</sub> were comparable for all catalysts. The catalysts became gradually deactivated due to accumulation of carbonaceous species on their surface [15,28,30].

Long-term activity, as well as CO<sub>x</sub> concentration, were determined for Mn10%-Co2.5% catalyst and the results are presented in Fig. 6. The conversions of acetone and ozone after 24 h at 25°C reached 55% and 43%, respectively. CO<sub>x</sub> concentrations and CO/CO<sub>2</sub> ratio remained almost unchanged within 24 h of reaction.

From the presented results, it can be understood that augmenting a single metal oxide catalyst improves its performance. However, the secondary metals at their lower loading of 2.5% or 5% resulted in better decomposition of ozone and higher rate of acetone oxidation. It has been reported that in catalytic ozonation process, ozone decomposition occurs on the catalyst and active oxygen species are formed which are responsible for VOC oxidation [11,14]. Reed et al. have studied the effect of metal oxide loading from 3% to 20% on MnO<sub>x</sub>/SiO<sub>2</sub> catalysts [14]. They have reported that lower oxidation states of higher loaded catalysts contribute to higher rate of acetone degradation. They suggested that when oxidation states of metal particles are lower, they could interact with ozone more easily to create active oxygen species. Einaga et al. [24] have investigated the structure of Mn oxides on

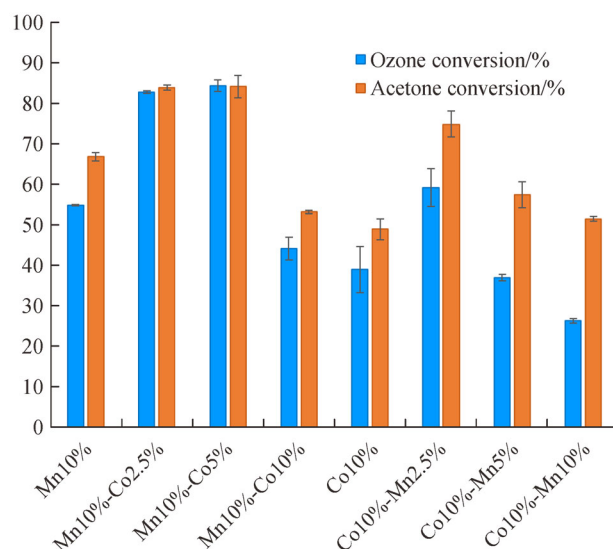


**Fig. 4** Acetone and ozone conversions (%) at 25°C and 150 min of reaction, [acetone] = 150 ppm, and [O<sub>3</sub>] = 1200 ppm, catalyst weight = 0.065 g, gas flow rate = 250 mL · min<sup>-1</sup>.

**Table 4** Catalytic activity of single and mixed metal oxides catalysts for acetone ozonation at 150 min of reaction <sup>a)</sup>

Catalyst	Acetone oxidation rate /( $\times 10^5$ mol · min <sup>-1</sup> · g <sup>-1</sup> )	Ozone decomposition rate /( $\times 10^5$ mol · min <sup>-1</sup> · g <sup>-1</sup> )	CO <sub>x</sub> yield /%
Mn10%/γ-Al <sub>2</sub> O <sub>3</sub>	1.57	11.26	91.31
Mn10%-Co2.5%/γ-Al <sub>2</sub> O <sub>3</sub>	1.98	17.01	90.41
Mn10%-Co5%/γ-Al <sub>2</sub> O <sub>3</sub>	1.98	17.34	90.53
Mn10%-Co10%/γ-Al <sub>2</sub> O <sub>3</sub>	1.25	9.07	92.98
Co10%/γ-Al <sub>2</sub> O <sub>3</sub>	1.15	8.00	95.71
Co10%-Mn2.5%/γ-Al <sub>2</sub> O <sub>3</sub>	1.76	12.16	88.21
Co10%-Mn5%/γ-Al <sub>2</sub> O <sub>3</sub>	1.35	7.60	91.48
Co10%-Mn10%/γ-Al <sub>2</sub> O <sub>3</sub>	1.21	5.39	96.58

a) [acetone] = 150 ppm, [O<sub>3</sub>] = 1200 ppm, catalyst weight = 0.065 g, gas flow rate = 250 mL · min<sup>-1</sup>, 25°C, Data were taken at 150 min of reaction.

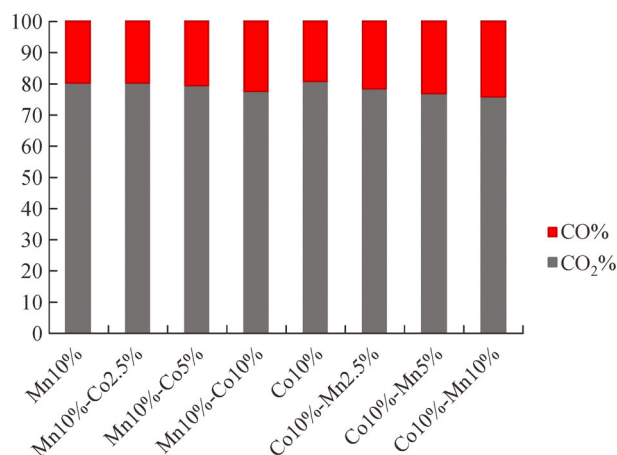


**Fig. 5** CO% and CO<sub>2</sub>% in the reaction product stream at 25°C and 150 min of reaction, [acetone] = 150 ppm, and [O<sub>3</sub>] = 1200 ppm, catalyst weight = 0.065 g, gas flow rate = 250 mL · min<sup>-1</sup>.

alumina in different metal loadings in ozonation of benzene. They have concluded that catalysts with lower loadings (1%–7.5%) have presented higher activities. Similar study by Rezaei et al. has found that catalysts with lower Mn oxidation states are more active in ozonation of toluene [12]. It has been reported that catalysts with lower metal loadings have lower oxidation state and are more active in transferring electrons to ozone to induce ozone decomposition reaction [12].

### 3.3 *In-situ* DRIFTS studies and reaction pathway

The *in-situ* DRIFTS spectra of four selected catalysts during the reaction are depicted in Fig. 7. According to Fig. 7(a–d), acetone is adsorbed on the catalysts. This can be confirmed by the characteristic acetone bands at 1371 and 1424–1427 cm<sup>-1</sup>. The peak at around 1702 cm<sup>-1</sup> (C=O stretching) and the broad band between 2400 and 3750 cm<sup>-1</sup> (OH stretching) were other detected bands. Appear-

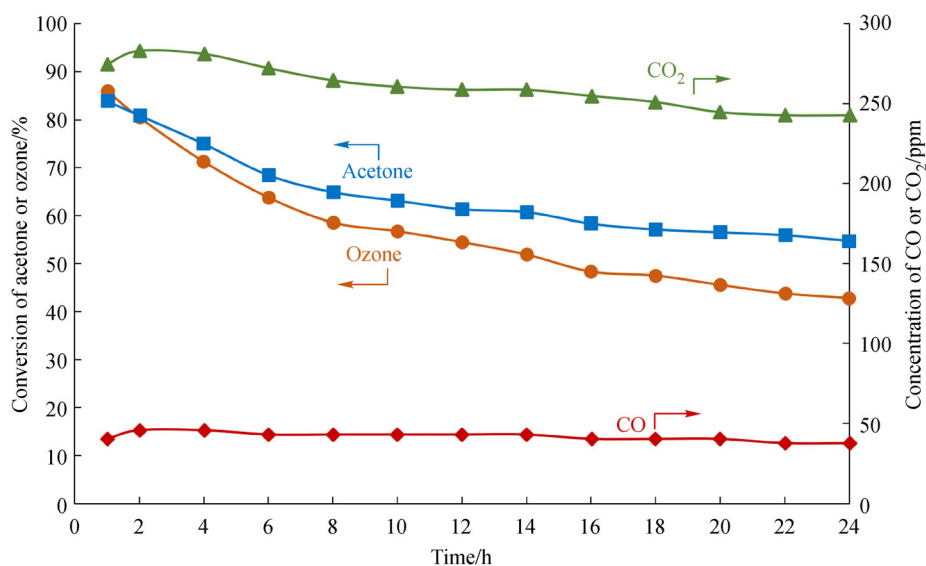


**Fig. 6** Long-term activity and product formation of Mn10%-Co2.5%/γ-alumina at 25°C, [acetone] = 150 ppm, and [O<sub>3</sub>] = 1200 ppm, catalyst weight = 0.065 g, gas flow rate = 250 mL·min<sup>-1</sup>.

ance of the peaks at 1590–1601 cm<sup>-1</sup> (COO<sup>-</sup> stretching of carboxylate species) confirmed adsorption of acetone which is partially oxidized to carboxylate groups [28,33,34]. A recent study has shown that in the presence of ozone, acetone is first oxidized to surface carboxylates; then, the surface carboxylates are further oxidized to alcohols, ketones, carboxylic acids, and eventually to carbon dioxide and carbon monoxide [28]. In a typical experimental run, after saturation of the catalyst with acetone, ozone was introduced into the system. New peaks appeared and the intensity of the characteristic peaks of acetone declined gradually as they are presented in the representative time spectra. As can be seen in Fig. 7, the main bands are at around 1410–1427 (C–H asymmetric deformation vibration), 1462–1468 (methyl and methylene C–H bending), 1580–1600 (antisymmetric and symmetric COO<sup>-</sup> stretching of carboxylates), 1700–1726 (C=O stretching of ketones and carboxylic acids), and 2700–3650 cm<sup>-1</sup> (OH stretching of alcohols, carboxylic acids, and water). The intensity of the bands increased over the time of reaction.

By comparing the spectra of the four catalysts in Fig. 7, it can be inferred that acetone degradation pathway is most probably the same for the alumina supported Mn10%, Co10%, Mn10%-Co2.5%, and Co10%-Mn2.5% catalysts. During adsorption of acetone, intensity of the peak at around 1600 cm<sup>-1</sup> was relatively weaker in Co10% than other catalysts. This can suggest that chemical adsorption was weaker in Co10%. However, the appeared peaks indicated that both chemical and physical adsorption occurred in all selected samples.

From the activity results discussed in Fig. 4 and Table 4, addition of Mn2.5% to Co-based catalyst and Co2.5% to Mn-based catalyst enhances the activity of the single metal

oxide catalysts. XANES and EXAFS studies indicate that the oxidation states and local structure of the primary metal does not change by addition of the secondary metal. Therefore, the secondary metal does not interact with the structure of the primary metal. As also can be observed in Fig. 7, the single Mn10% and Co10% have similar spectra and it can be assumed that reaction pathway on these two metals are the same.

It has been reported that ozone is decomposed on the surface of metal oxide catalysts to form atomic oxygen and peroxide species (Eqs. (3–6)). These studies have been carried out on supported manganese oxides [14,24,30] as well as cobalt oxides [23].



where  $\blacksquare$  refers to surface of metal active sites. Reed et al. studied catalytic ozonation of acetone over silica-supported Mn oxides with Mn loading from 3% to 20% [31]. They proposed that almost all the adsorbed acetone on the catalyst are located on silica sites. Therefore, silica acts as a reservoir for the acetone, which is physically adsorbed on the catalyst. Then, the adsorbed acetone molecules migrate to the Mn sites and react with active atomic oxygen. In another study on ozonation of acetone using alumina supported Mn oxides, it has been suggested by Aghbolaghy et al. that alumina is not an inert support. Alumina acts as reservoir for adsorbed acetone, and it also interacts with acetone to create surface carboxylate intermediates [28]. The role of alumina for catalytic ozonation of acetone was

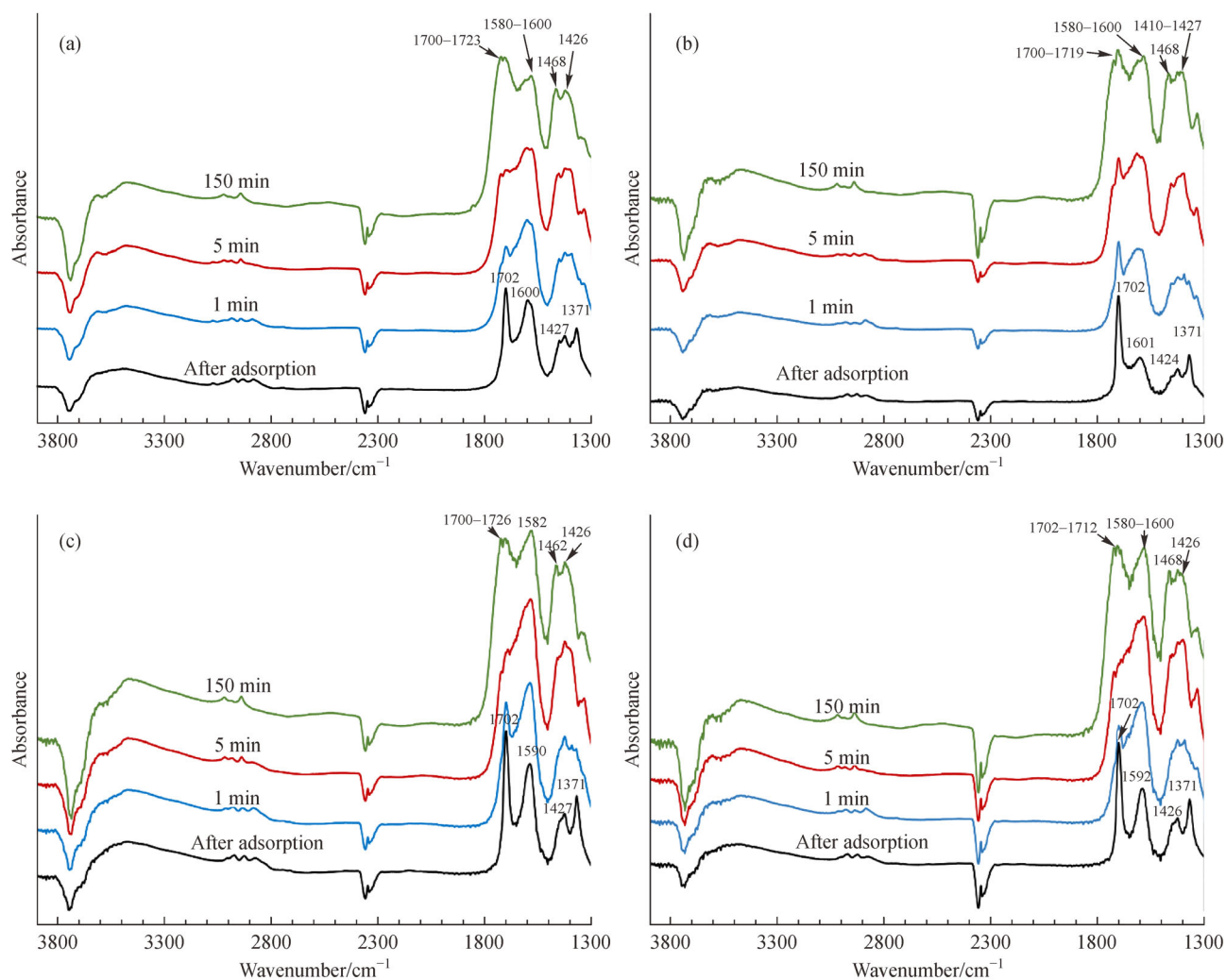


**Fig. 7** DRIFTS spectra of catalytic ozonation of acetone at 25°C using alumina supported (a) Mn10%, (b) Co10% , (c) Mn10%-Co2.5%, and (d) Co10%-Mn2.5%; [acetone] = 150 ppm, [O<sub>3</sub>] = 1200 ppm, catalyst weight = 0.065 g, gas flow rate = 250 mL · min<sup>-1</sup>.

studied by performing the reaction on pure alumina. Alumina alone was unable to oxidize the surface carboxylates that were formed, and Mn sites were essential for completing the oxidation process. According to *in-situ* DRIFTS results, the presence of similar bands for Mn10% and Co10% catalyst suggest that both Mn and Co catalysts follow the same reaction pathway. In the case of Mn and Co mixed oxides, the intensity of the appeared peaks becomes stronger indicating the role of both metals in forming surface carboxylates in the reaction. It has been reported that lower oxidation states of Mn are preferable for ozonation of VOCs. This reason is attributed to the ability of Mn atoms in lower loaded sample in transferring electron to ozone [12,14]. In a similar research on supported Co oxide catalyst, enhanced activity of lower loading samples was related to increase in dispersion and decrease in oxidation state of cobalt which resulted in improved electron transferring ability and ozone utilization

[23]. Therefore, lower oxidation states of Mn and Co in this work can enhance the ozone decomposition reaction and consequently the oxidation rate of VOCs.

In the presence of both Mn and Co sites, the surface carboxylates are oxidized to carboxylic acids, alcohols, and ketones, and eventually to CO and CO<sub>2</sub>. According to the findings of this work and the results of the previous studies [28,35], it can be concluded that alumina, Mn, and Co are playing roles in ozone decomposition to create highly reactive atomically adsorbed oxygen species in the proposed mechanism. The incomplete oxidation of acetone and formation of undesired products accumulated on the catalysts cause gradual deactivation of the catalyst at 25°C [28].

Based on the above discussion, the observed differences in the catalytic performance are due to structural differences between the catalysts. It has been reported by Einaga et al. that surface area plays an import role in

increasing the catalyst activity in ozonation of benzene [15]. They found that irrespective of the type of the catalyst support, there is a linear relationship between specific surface area and reaction rate. In this work, it can be seen that by adding higher content of metal oxides on the support, the surface area decreases slightly. Although the activity of the catalyst increased considerably in Mn10%-Co2.5% and Co10%-Mn2.5% catalysts compared to single Mn10% and Co10%, the surface area decreased. Therefore, it can be deduced that surface area cannot justify the enhancement in catalyst activity.

On the other hand, researchers have reported the impact of metal loading on the oxidation state of metal and eventually catalyst activity [12,14,23]. Findings of this work also suggest the same conclusion about the effect of lower oxidation states on higher acetone conversion. In both alumina supported Mn and Co-based catalysts, by decreasing the loading of the secondary metal to 2.5%, its oxidation state decreased which led to higher conversions. It is suggested that Mn<sub>3</sub>O<sub>4</sub> (mixed Mn oxidation state of +3 and +2) and CoO (oxidation state of +2) are the most active species among the observed Mn and Co phases. Mn<sub>3</sub>O<sub>4</sub> and CoO constitute 20% and 45% of the Mn and Co species in Mn10%-Co2.5% catalyst respectively, while Mn10% catalyst contains only 7% Mn<sub>3</sub>O<sub>4</sub> and Co10% catalyst contains no CoO. The catalysts containing higher amounts of CoO and Mn<sub>3</sub>O<sub>4</sub> performed better than other catalysts.

## 4 Conclusions

Catalytic ozonation of acetone over a series of alumina supported single and mixed transition metal oxide catalysts was studied at room temperature. All catalysts lost their activity gradually at room temperature due to accumulation of intermediates on their surface. It was shown that addition of lower loading of the secondary metal to Co and Mn catalysts improved activity of the catalysts. By augmenting the catalyst with the second metal, the local structure and oxidation state of the primary metal remained the same. However, by changing the loading of the secondary metals, its oxidation state changed. It was suggested that activity of the catalysts is related to the metal's oxidation state and lower metal loadings (5 wt-% or less) result in lower oxidation states. Catalysts having lower oxidation states are more active in transferring electrons to ozone, leading to higher ozone decomposition, and thus enhanced acetone oxidation.

**Acknowledgements** Authors would like to thank the University of Saskatchewan and the Natural Sciences and Engineering Research Council of Canada for their financial support of this research. XANES and EXAFS were performed at the Canadian Light Source, which is supported by the Canada Foundation for Innovation, the Natural Sciences and Engineering Research Council of Canada, the University of Saskatchewan, the Government of Saskatchewan, Western Economic Diversification Canada,

the National Research Council Canada, and the Canadian Institutes of Health Research.

## References

- Bastos S S, Carabineiro S A, Órfão J J, Pereira M F, Delgado J J, Figueiredo J L. Total oxidation of ethyl acetate, ethanol and toluene catalyzed by exotemplated manganese and cerium oxides loaded with gold. *Catalysis Today*, 2012, 180(1): 148–154
- Bo L, Sun S. Microwave-assisted catalytic oxidation of gaseous toluene with a Cu-Mn-Ce/cordierite honeycomb catalyst. *Frontiers of Chemical Science and Engineering*, 2019, 13(2): 385–392
- Wang Z, Zhou J, Zhu Y, Wen Z, Liu J, Cen K. Simultaneous removal of NO<sub>x</sub>, SO<sub>2</sub> and Hg in nitrogen flow in a narrow reactor by ozone injection: Experimental results. *Processing Technology*, 2007, 88(8): 817–823
- Ma Q, Wang Z, Lin F, Kuang M, Whiddon R, He Y, Liu J. Characteristics of O<sub>3</sub> oxidation for simultaneous desulfurization and denitration with limestone-gypsum wet scrubbing: Application in a carbon black drying kiln furnace. *Energy & Fuels*, 2016, 30(3): 2302–2308
- Rezaei F, Moussavi G, Bakhtiari A R, Yamini Y. Toluene removal from waste air stream by the catalytic ozonation process with MgO/GAC composite as catalyst. *Journal of Hazardous Materials*, 2016, 306: 348–358
- Teramoto Y, Kosuge K, Sugawara M, Kim H H, Ogata A, Negishi N. Zirconium/cerium oxide solid solutions with addition of SiO<sub>2</sub> as ozone-assisted catalysts for toluene oxidation. *Catalysis Communications*, 2015, 61: 112–116
- Wang Q, Tang M, Peng Y, Du C, Lu S. Ozone assisted oxidation of gaseous PCDD/Fs over CNTs-containing composite catalysts at low temperature. *Chemosphere*, 2018, 199: 502–509
- Huang H, Ye X, Huang W, Chen J, Xu Y, Wu M, Shao Q, Peng Z, Ou G, Shi J, Feng X, Feng Q, Huang H, Hu P, Leung D Y C. Ozone-catalytic oxidation of gaseous benzene over MnO<sub>2</sub>/ZSM-5 at ambient temperature: Catalytic deactivation and its suppression. *Chemical Engineering Journal*, 2015, 264: 24–31
- Lin F, Wang Z, Ma Q, Yang Y, Whiddon R, Zhu Y, Cen K. Catalytic deep oxidation of NO by ozone over MnO<sub>x</sub> loaded spherical alumina catalyst. *Applied Catalysis B: Environmental*, 2016, 198: 100–111
- Xi Y, Reed C, Lee Y K, Oyama S T. Acetone oxidation using ozone on manganese oxide catalysts. *Journal of Physical Chemistry B*, 2005, 109(37): 17587–17596
- Einaga H, Teraoka Y, Ogata A. Catalytic oxidation of benzene by ozone over manganese oxides supported on USY zeolite. *Journal of Catalysis*, 2013, 305: 227–237
- Rezaei E, Soltan J, Chen N. Catalytic oxidation of toluene by ozone over alumina supported manganese oxides: Effect of catalyst loading. *Applied Catalysis B: Environmental*, 2013, 136-137: 239–247
- Aghbolaghy M, Soltan J, Chen N. Low temperature catalytic oxidation of binary mixture of toluene and acetone in the presence of ozone. *Catalysis Letters*, 2018, 148(11): 3431–3444
- Reed C, Lee Y K, Oyama S T. Structure and oxidation state of silica-supported manganese oxide catalysts and reactivity for acetone

- oxidation with ozone. *Journal of Physical Chemistry B*, 2006, 110 (9): 4207–4216
15. Einaga H, Ogata A. Benzene oxidation with ozone over supported manganese oxide catalysts: Effect of catalyst support and reaction conditions. *Journal of Hazardous Materials*, 2009, 164(2-3): 1236–1241
  16. Liu X, Zeng J, Shi W, Wang J, Zhu T, Chen Y. Catalytic oxidation of benzene over ruthenium-cobalt bimetallic catalysts and study of its mechanism. *Catalysis Science & Technology*, 2017, 7(1): 213–221
  17. Fiorenza R, Crisafulli C, Condorelli G G, Lupo F, Scire S. Au-Ag/CeO<sub>2</sub> and Au-Cu/CeO<sub>2</sub> catalysts for volatile organic compounds oxidation and CO preferential oxidation. *Catalysis Letters*, 2015, 145(9): 1691–1702
  18. Barakat T, Idakiev V, Cousin R, Shao G S, Yuan Z Y, Tabakova T, Siffert S. Total oxidation of toluene over noble metal based Ce, Fe and Ni doped titanium oxides. *Applied Catalysis B: Environmental*, 2014, 146: 138–146
  19. Konova P, Stoyanova M, Naydenov A, Christoskova S, Mehandjiev D. Catalytic oxidation of VOCs and CO by ozone over alumina supported cobalt oxide. *Applied Catalysis A, General*, 2006, 298: 109–114
  20. Liotta L F, Ousmane M, Di Carlo G, Pantaleo G, Deganello G, Marci G, Retailleau L, Giroir-Fendler A. Total oxidation of propene at low temperature over Co<sub>3</sub>O<sub>4</sub>-CeO<sub>2</sub> mixed oxides: Role of surface oxygen vacancies and bulk oxygen mobility in the catalytic activity. *Applied Catalysis A, General*, 2008, 347(1): 81–88
  21. Zhao Q, Liu Q, Song C, Ji N, Ma D, Lu X. Enhanced catalytic performance for VOCs oxidation on the CoAlO oxides by KMnO<sub>4</sub> doped on facile synthesis. *Chemosphere*, 2019, 218: 895–906
  22. Deganello G, Giannici F, Martorana A, Pantaleo G, Prestianni A, Balerna A, Liotta L F, Longo A. Metal-support interaction and redox behavior of Pt(1 wt-%)/Ce<sub>0.6</sub>Zr<sub>0.4</sub>O<sub>2</sub>. *Journal of Physical Chemistry B*, 2006, 110(17): 8731–8739
  23. Aghbolaghy M, Ghavami M, Soltan J, Chen N. Effect of active metal loading on catalyst structure and performance in room temperature oxidation of acetone by ozone. *Journal of Industrial and Engineering Chemistry*, 2019, 77: 118–127
  24. Einaga H, Harada M, Ogata A. Relationship between the structure of manganese oxides on alumina and catalytic activities for benzene oxidation with ozone. *Catalysis Letters*, 2009, 129(3-4): 422–427
  25. Einaga H, Maeda N, Teraoka Y. Effect of catalyst composition and preparation conditions on catalytic properties of unsupported manganese oxides for benzene oxidation with ozone. *Applied Catalysis B: Environmental*, 2013, 142-143: 406–413
  26. Yao X, Li Y, Fan Z, Zhang Z, Chen M, Shangguan W. Plasma catalytic removal of hexanal over Co-Mn solid solution: Effect of preparation method and synergistic reaction of ozone. *Industrial & Engineering Chemistry Research*, 2018, 57(12): 4214–4224
  27. Ravel B, Newville M. ATHENA, ARTEMIS, HEPHAESTUS: Data analysis for X-ray absorption spectroscopy using IFEFFIT. *Journal of Synchrotron Radiation*, 2005, 12(4): 537–541
  28. Aghbolaghy M, Soltan J, Sutarto R. The role of surface carboxylates in catalytic ozonation of acetone on alumina-supported manganese oxide. *Chemical Engineering Research & Design*, 2017, 128: 73–84
  29. Solsona B, Davies T E, Garcia T, Vázquez I, Dejoz A, Taylor S H. Total oxidation of propane using nanocrystalline cobalt oxide and supported cobalt oxide catalysts. *Applied Catalysis B: Environmental*, 2008, 84(1-2): 176–184
  30. Rezaei E, Soltan J. Low temperature oxidation of toluene by ozone over MnO<sub>x</sub>/γ-alumina and MnO<sub>x</sub>/MCM-41 catalysts. *Chemical Engineering Journal*, 2012, 198-199: 482–490
  31. Reed C, Xi Y, Oyama S T. Distinguishing between reaction intermediates and spectators: A kinetic study of acetone oxidation using ozone on a silica-supported manganese oxide catalyst. *Journal of Catalysis*, 2005, 235(2): 378–392
  32. Borodziński A, Bonarowska M. Relation between crystallite size and dispersion on supported metal catalysts. *Langmuir*, 1997, 13 (21): 5613–5620
  33. Hernández-Alonso M D, Tejedor-Tejedor I, Coronado J M, Anderson M A, Soria J. Operando FTIR study of the photocatalytic oxidation of acetone in air over TiO<sub>2</sub>-ZrO<sub>2</sub> thin films. *Catalysis Today*, 2009, 143(3-4): 364–373
  34. Li J, Na H, Zeng X, Zhu T, Liu Z. *In situ* DRIFTS investigation for the oxidation of toluene by ozone over Mn/HZSM-5, Ag/HZSM-5 and Mn-Ag/HZSM-5 catalysts. *Applied Surface Science*, 2014, 311: 690–696
  35. Aghbolaghy M, Soltan J, Chen N. Role of surface carboxylates in the gas phase ozone-assisted catalytic oxidation of toluene. *Catalysis Letters*, 2017, 147(9): 2421–2433